Research Square

Preprints are preliminary reports that have not undergone peer review.
They should not be considered conclusive, used to inform clinical practice,
or referenced by the media as validated information.

# SART1 localizes to spindle poles forming a SART1 cap and promotes centrosome and spindle assembly

**Hideki Yokoyama** ( hyokoyama@gm.ibaraki-ct.ac.jp )
National Institute of Technology, Ibaraki College https://orcid.org/0000-0002-0157-954X
**Kaoru Takizawa**
ID Pharma
**Jian Ma**
ID Pharma
**Daniel Moreno-Andrés**
RWTH Aachen University
**Wolfram Antonin**
RWTH Aachen https://orcid.org/0000-0003-4669-379X
**Yoshikazu Haramoto**
National Institute of Advanced Industrial Science and Technology (AIST)

**Article**

**Keywords:** cancer, centrosomal protein, microtubule binding, mitotic cell death, spindle pole formation, Ran

**Posted Date:** January 13th, 2021

**DOI:** https://doi.org/10.21203/rs.3.rs-126500/v1

**License:** This work is licensed under a Creative Commons Attribution 4.0 International License.
Read Full License

# Abstract

SART1 is overexpressed in various cancers. However, its physiological function and cancer relevance remains elusive. Here we identify SART1 as a mitotic-specific and Ran-regulated microtubule-associated protein. SART1 downregulation in human cells as well as its depletion from frog egg extracts disrupts spindle assembly. While SART1 is nuclear in interphase, it localizes during mitosis to spindle poles in a microtubule-dependent manner. SART1 accumulates close to centrosomes forming a half circle which we designate as SART1 cap. Immunoprecipitation of SART1 identifies the centrosome scaffold protein Cep192 as an interaction partner. Accordingly, Cep192 downregulation abolishes SART1 localization to spindle poles, and SART1 downregulation displaces centrosomal proteins like Ninein from centrosomes, but does not affect γ-tubulin localization. Furthermore, SART1 downregulation selectively kills cancer cells and prevents normal cells from oncogenic transformation. Our data unravel a novel function of SART1 for centrosome organization and spotlight SRAT1 as a potential target for anticancer therapies.


# Introduction

The squamous cell carcinoma antigen recognized by T-cells 1 (SART1) gene was first identified and cloned as a carcinoma antigen recognized by cytotoxic T-cells[1]. Indeed, the SART1 protein is expressed in most proliferating cells and is especially overexpressed in cancer cells including epithelial cancers[2]. Therefore, SART1 has been considered as a potential diagnostic marker and therapeutic target in various cancers[3,4]. However, it is still unknown whether SART1 overexpression is a cause or a consequence of malignant cell transformation and the physiological function of SART1 remains elusive.

In cell free assays using HeLa cell nuclear extracts, SART1 is required for U4/U6.U5 tri-snRNP recruitment to the pre-spliceosome in the spliceosome assembly pathway and plays a role in pre-mRNA splicing[5]. Therefore, SART1 is also called as U4/U6.U5 tri-snRNP-associated protein 1. In addition, SART1 was identified in genome wide RNAi screenings as one of the genes required for mitotic progression[6,7]. Specific RNAi screens found SART1 as critical factor for centriole biogenesis[8] and sister chromatid cohesion[9]. Furthermore, SART1 knockout in mice is embryonic lethal[10]. All this suggest that SART1 has crucial functions in mitosis and cell division with vital importance for organismic homeostasis and/or development. However, we still lack detailed knowledge about the molecular action of SART1 in mitosis.

In eukaryotic cells, proteins containing nuclear localization signal (NLS) reside inside the nucleus in interphase with critical nuclear functions, including DNA replication, transcription, and splicing. Upon nuclear envelope breakdown at the beginning of mitosis, however, nuclear proteins become accessible to cytoplasmic proteins, including microtubules (MTs), and can play time-specific, moonlighting roles for spindle assembly and function[11]. Also, many of the nuclear proteins specifically function in the vicinity of mitotic chromatin, because of the GTP-bound form of the Ran GTPase (RanGTP) produced locally around chromatin[12]. RanGTP binds to the heterodimeric nuclear transport receptor importin α/β and dissociates NLS-containing nuclear proteins from the importins. The liberated nuclear proteins are active

and induce spindle assembly around chromatin. To identify such nuclear MT regulators, we have affinity-purified NLS-containing proteins and MT-associated proteins (MAPs) sequentially, and obtained over 200 proteins[13,14]. The NLS-MAPs has been proven to be an excellent resource to uncover new mitotic regulators and reveal their functions[15,16].

One of the NLS-MAPs is SART1, a so far unrecognized MAP that uniquely localizes to spindle poles. We show here that SART1 is required for mitotic progression and spindle assembly. The SART1 function at the spindle pole involves its interaction with Cep192 and recruitment of some centrosomal proteins.

# Results

### SART1 is a bona-fide microtubule-associated protein.

To test whether SART1 can indeed interact with MTs, we added taxol-stabilized MTs to HeLa nuclear extracts. Endogenous SART1 was efficiently co-sedimented, which indicates its MT binding (Fig 1A). Addition of recombinant importin a/b complex inhibited SART1-MT interaction (Fig 1A). Inhibition was reversed by the co-addition of RanGTP, which binds to importin b and removes the importin complex from NLS-sites. As previously reported, the MT polymerase chTOG, the orthologue of Xenopus XMAP215, showed no inhibition by importins[16]. Similarly, SART1 was co-sedimented from Xenopus egg extracts with taxol-stabilized MTs (Fig S1A).

To examine whether SART1 directly interacts with MTs, we expressed recombinant Xenopus SART1 in bacteria, using an Acidic-Target Tag[17] for better solubility. In MT sedimentation assay, recombinant SART1 directly bound to MTs (Fig. S1B). This MT binding was inhibited by importin a/b and restored by further addition of RanGTP (Fig. S1C). These results indicated that SART1 is a bona-fide, previously unrecognized, MAP, which is regulated by importins and RanGTP.

### SART1 is required for mitotic progression and spindle assembly.

To assess SART1 impact on mitosis, we knocked down SART1 in HeLa cells by RNA interference (RNAi). SART1 expression was efficiently down-regulated with three independent small-interfering RNA (siRNA) oligos (Fig S2A). Live cell imaging of HeLa cells stably expressing histone H2B-mCherry was carried out with 3 min time frame (Fig 1B), and the imaging data was automatically analyzed using the CellCognition software[16,18]. Upon SART1 depletion, we found a significant delay of prometaphase progression and often saw that chromosomes do not properly align to the metaphase plate (Fig 1B and C). For further detailed characterization of SART1, we used siSART1#3 oligo, if not stated otherwise, because this oligo induces milder spindle defects and less cell death compared to the other two (Fig. S2A-C and S3C).

Immunostaining of the fixed siSART1#3-treated cells showed consistently chromosome misalignments and also spindle MT defects (Fig 1D and E). MTs appeared not tightly arranged inside the spindle, and spindle poles were not well focused. Similar spindle defects were observed with all of the three siRNAs (Fig. S2B). In agreement, we found by FACS analysis that SART1 depletion significantly induces apoptotic

cell death (Figs. S2C and S3). Detail analysis of the live cell imaging data revealed that a considerable number of cells die as consequence of early mitotic defects (Fig. S3).

To further validate that the spindle defects are caused by the lack of SART1, we performed rescue experiments. We used a Sendai virus (SeV) vector system to transiently express a SART1 version resistant to downregulation by siSART1#3 oligo[19] (Fig S2D). Indeed, the exogenous SART1 was well expressed in HeLa cells and fully rescued the spindle defects (Fig. 1 D-F).

**Chromosome attachment defects and spindle checkpoint activation in SART1-depleted cells.**

To understand the nature of the spindle defects, we immunostained SART1-depleted cells for the kinetochore marker CREST. In control cells, kinetochore pairs were connected to MTs emanating from both spindle poles with end-on attachment (Fig. 1G). In contrast, in SART1 depleted cells we could not detect clear MT-kinetochore interactions (Fig. 1G). Functional end-on attachments are known to generate tension to separate kinetochores of sister chromatids, increasing the interkinetochore distance. We co-stained the cells for CREST and CENP-A, a histone H3 variant incorporated in centromeric DNA, and measured the distance of two CENP-A dots. Whereas control cells showed an inter-kinetochore distance of 1.1 μm, in SART1 depleted cells the distance was reduced to 0.8 μm (Fig. 1H). Staining with an outer kinetochore marker Ndc80/Hec1 also showed shorter interkinetochore distance upon SART1 downregulation (Fig. S2E). Consistently, the mitotic checkpoint protein BubRI remains localized at the metaphase spindle (Fig. S2G), indicating activation of the spindle checkpoint in the absence of SART1.These results indicate that SART1 is required for establishing and/or maintaining MT-kinetochore attachment and suggest that sister chromatides remain connected upon SART1 downregulation. Indeed, on chromosome spreads, we observed proper sister chromatid cohesion, at least in our depletion condition (Fig. S2F).

**SART1 localizes near centrosomes in the presence of dynamic microtubules.**

To understand the place where SART1 functions, we examined the localization of SART1 in HeLa cells. A human SART1 antibody stained the nucleus and partially the cytoplasm in interphase cells (Fig. 2A) as reported[20], but surprisingly labeled the spindle poles in mitosis (Fig. 2B). This staining is specific because it was lost upon SART1 downregulation (Fig. 2A and B). After nuclear envelope breakdown, SART1 partially localized to the centers of two MT asters at prophase and accumulated further to the arising spindle poles at prometaphase (Fig. S4A). The spindle pole localization was most prominent in metaphase, remained through early anaphase and disappeared in telophase (Fig. S4A).

The major component of spindle pole is a centrosome that functions as the primary MT-organizing center. It consists of two centrioles surrounded by the pericentriolar material (PCM). When costained with a PCM marker γ-tubulin, SART1 localized around γ-tubulin in early mitosis, but interestingly formed a half circle around the γ-tubulin facing away from the spindle axis (Fig. 2C). The SART1 signal was similarly detected as a half circle around another PCM marker, pericentrin (Fig. 2D). This SART1-pericentrin configuration was also observed using a different SART1 antibody (SART1 #2) (Fig. S4B).

Given the identification of SART1 as a MAP, we examined how MTs affect the spindle pole localization of SART1. Before fixation, HeLa cells were treated for 10 min with taxol to stabilize MTs or with nocodazole to depolymerize MTs. In both conditions, SART1 disappeared from the spindle poles (Fig. 2E), indicating a requirement of dynamic MTs for the SART1 localization. This contrasts to the pole localization of γ-tubulin which is not displaced by taxol or nocodazole treatment (Fig. S4C). These results indicate that SART1 localizes to the distal surface of centrosomes along the spindle axis and that this localization is dependent on dynamic MTs.

## SART1 interacts with Cep192, which promotes the pole accumulation of SART1.

To understand the mechanism of how SART1 localizes near centrosomes, we immunoprecipitated endogenous SART1 from Xenopus egg extracts using a specific antibody we generated (Fig. 3A and S5A). SART1-interacting proteins were eluted from the antibody beads with a high pH buffer (Fig. S5B), while SART1 remained mostly on the beads (Fig. S5B) presumably due to strong antigen-antibody interaction. Analysis of the eluate by shotgun mass spectrometry identified known interacting partners of SART1 involved in mRNA splicing, for example SF3B3 (Table S1). As expected, SART1 itself was found with low score (quantitative value 1).

Intriguingly, mass spectrometry identified a number of centrosomal proteins, containing Centrosomal protein of 192 kDa (Cep192) with the third highest score (Table S1, quantitative value 92). Cep192 is an integral component of centrosomes regulating recruitment of many centrosomal proteins and is required for centriole duplication and centrosome maturation[21,22]. To confirm the SRAT1-Cep192 interaction, we reciprocally immunoprecipitated Cep192 from HeLa cell lysate using a commercial antibody. Although in our hand we could not detect Cep192 band by Western blot, we found SART1 in the Cep192 precipitates (Fig. 3B). Co-staining of the two proteins showed that SART1 localizes in proximity to Cep192, with SART1 covering the distal surface of the Cep192 spots in metaphase (Fig.3C).

When Cep192 was depleted in HeLa cells with an established siRNA[23], SART1 are was undetectable at spindle poles (Fig. 3D). Yet, SART1 protein levels were unchanged upon Cep192 depletion (Fig. 3E), indicating that Cep192 is required for accumulation of SART1 on spindle poles but not for its stability. In contrast, SART1 depletion resulted in only partial (~30%) reduction of Cep192 staining at mitotic centrosomes (Fig. 3F and G). While we do not know protein level of Cep192 in the absence of SART1, we confirmed that mRNA level of Cep192 unchanged in the absence of SART1 (Fig. S5C). We conclude that Cep192 is a interaction partner of SART1 critically required for SART1 accumulation near mitotic centrosomes. In contrast, SART1 partially increases Cep192 levels at centrosomes.

## SART1 is required for recruitment of centrosomal proteins, throughout the cell cycle.

Since SART1 accumulates near mitotic centrosomes and interacts with centrosomal proteins, we examined the localization of other key centrosomal components upon SART1 depletion. The staining intensity of the MT anchoring protein Ninein[24] at centrosomes decreased in mitosis but surprisingly also in interphase (Fig. 4A), upon SART downregulation using three different SART1 siRNAs. The centrosome

staining of the scaffolding protein pericentrin was also decreased throughout the cell cycle (Fig. S6A), but in this case the reduction in interphase was even more prominent (Fig. S6A). The staining of the centriolar satellite protein PCM1, also present in the SART1 immunoprecipitates (quantitative value 11), was dispersed both in mitosis and interphase (Fig. 4B) upon SART1 downregulation. We quantified this phenotype by measuring centrosomal versus cytoplasmic staining intensity of PCM1 (Fig. 4B), which showed PCM1 mislocalization both in interphase and mitosis. Similarly, EB1, a MT plus-end binding protein known to localize to centrosomes [25], also showed reduced staining at mitotic and interphase centrosomes in SART1-depleted cells (Fig. 4C) indicating a less efficient EB1 recruitment to centrosomes. Total EB1 protein level were unchanged upon SART1 downregulation (Fig.S2), indicating inhibition of EB1 recruitment to centrosomes. Also, mRNA levels of Ninein, Pericentrin, and PCM1 were not reduced in the absence of SART1 (Fig. S6B).

Reduction of centrosomal protein localization in interphase could indicate altered MT functions. MTs regulate cell polarization and migration in interphase[26]. We thus tested these functions using an in vitro wound healing assay. siSART1-treated U2OS cells showed clear reduction of cell migration (Fig. 4D) pointing to a role of SART1 also for interphase MT function.

Whereas centrosome accumulation of Ninein, pericentrin, PCM1 and EB1 was impeded by SART1 downregulation, recruitment of γ-tubulin, a primary MT nucleating factor, was not affected (Fig. S6C). This is different to the phenotype observed upon Cep192 downregulation which prevents γ-tubulin centrosome localization[21]. Also, distinct from Cep192[22], depletion of SART1 did not affect the number of centrioles, labeled with Centrin, at the spindle poles (Fig. S6D. Thus, SART1 is required to recruit selected proteins to the centrosome throughout the cell cycle, but this function is likely independent of Cep192.

**SART1 promotes spindle bipolarity in Xenopus egg extract via its N-terminal NLS-containing region.**

To further understand the molecular function of SART1, we used Xenopus egg extracts. In this cell-free system, spindle assembly can be faithfully recapitulated when sperm heads are added to the extracts and cell cycle activation is trigged into interphase and then to mitosis. SART1 antibody, used for the immunoprecipitation (Fig. 3A), efficiently depleted endogenous SART1 from egg extracts (Fig. 5A). Whereas control-treated (mock) extracts assembled bipolar spindles with chromosomes aligned at the metaphase plate, depletion of SART1 caused defects in spindle assembly (Fig.5B). Although MT polymerization around sperm chromatin was equivalent to the control situation, bipolar spindle orientation was not established and chromosomes did not align to the center (Fig.5B, C, and E). These spindle phenotypes were rescued by addition of Xenopus SART1 mRNA to express recombinant SART1 (Fig. 5A, B, and E).

To understand which parts of SART1 are crucial for its spindle function we constructed N- and C-terminal deletion mutants of the protein (Fig. 5D) and expressed them in SART1 depleted egg extracts (Fig. 5E). Besides the full-length SART1, the fragment lacking the last hundred aa at C-terminus (aa1-665) restored bipolar spindle assembly (Fig. 5E). In contrast, mutants lacking N-terminus did not, which suggests that a

potential NLS (aa 26-46 of Xenopus SART1, predicted by cNLS Mapper[27]) in the N-terminus might be important for MT binding and spindle bipolarization.

### SART1 depletion induces spindle defects in cancer cells, but not in normally growing cells

Because SART1 has been implicated in tumorigenesis[3,4] we overexpressed SART1 or an oncogene c-Myc[28] in non-transformed diploid retinal pigment epithelial 1 (RPE1) cells using SeV vector carrying SART1 (Fig. S2E) or c-Myc. After 1 month with occasional medium changes, control and SART1-expressed cells grew in a monolayer and stopped further growth due to contact inhibition[29], while c-Myc-expressed cells grew infinitely, became smaller, and formed multilayered colonies (Fig. S7A)[28]. The result suggests that SART1 is not a cause of tumorigenesis.

Next, we downregulated SART1 expression in normal and cancer cell lines. siSART1 treatment similarly downregulated SART1 in normal BJ skin fibroblasts and RPE cells, as well as in osteosarcoma-derived U2OS cells (Fig. 6A). Immunostaining indicated that SART1 depletion induces spindle and chromosome alignment defects only in U2OS cells (Fig. 6B, C, and S7B). Consistently, SART1-depleted RPE1 cells did not show increased apoptotic cell death (Fig. S7B), whereas SSX2IP depletion, which induces spindle defects in RPE1 cells[30], induced cell death (Fig. S7C).

RPE1 and BJ have an elongated cell shape, distinct from round morphology of cancer-derived HeLa and U2OS cells, and these cultures contain a lower fraction of mitotic cells than HeLa and U2OS cell cultures[31]. To examine whether these differences affect cell response to SART1 depletion, we used iPS (induced pluripotent stem) cells as non-cancerous cells with a high mitotic index[32,33]. Efficient SART1 downregulation in iPS cells neither affected spindle assembly nor caused cell death (Fig. 6D).

These experiments indicate that upon SART1 depletion, the cancer cell lines show a higher rate of cell death as compared to the normal cell lines. To examine if cell transformation changes their response to SART1 depletion, we downregulated SART1 expression in RPE1 cells and transformed them by c-Myc expression using the SeV vector carrying c-Myc. Cells were cultured for total 2 weeks with siRNA/medium change every 3 day. As expected, control RPE1 cells stopped growing while c-Myc-transformed cells grew infinitely (Fig. 6E). Interestingly, SART1 downregulation strikingly inhibited c-Myc-induced cell transformation without affecting control cells (Fig. 6E and S7D). This result, together with no cell death induced in SART1-depleted RPE1 cells (Fig. S7), indicates that SART1 downregulation preferentially induces cell death in transformed cells.

## Discussion

SART1 has been previously identified in RNAi screenings as a protein required for mitotic progression[6,7]. It was also found in a RNAi screening searching for proteins required for centrosome biogenesis[8]. However, mitotic and centrosomal function of SART1 has not been characterized in detail and it remained unclear whether SART1 is required for those events directly or indirectly via pre-mRNA splicing of relevant factors.

Here we demonstrate SART1 as a bona fide RanGTP-regulated MAP. SART1 localizes next to centrosomes and is required for centrosome maturation and spindle assembly. Some splicing factors (Cdc5l and the Cdc5l-containing Prp19 complex) have been shown to be important for spindle assembly[34,35]. Although these proteins do not localize to specific mitotic structures, their functions on spindle assembly are independent of mRNA splicing[35]. Thus, our data together with previous evidence support the idea that multiple splicing factors have moonlighting functions in mitosis[11].

SART1 has been described as one of the pre-mRNA splicing factors required for sister chromatid cohesion[9]. We show, however, by chromosome spreads that SART1-depleted cells exhibit proper sister chromatid cohesion. SART1 depletion also causes chromosome misalignment with reduced interkinetochore distance. This is distinct from the phenotype of cohesin component depletion which results in longer interkinetochore distances[36]. Both results indicate that sister chromatid cohesion is normal, at least under our depletion condition. Therefore, potential SART1 cohesion functions are unlikely to cause the spindle and centrosome assembly defects we observed.

SART1 resides inside of nucleus in interphase and is during his stage of the cell cycle undetectable at centrosomes. Upon nuclear envelope breakdown, SART1 starts accumulating around the two centrosomes and further increases in prometaphase. As bipolar spindles establish during metaphase, SART1 forms a half circle around centrosomes averted from the spindle axis. The SART1 localization near centrosomes is dependent on the presence of dynamic MTs, suggesting that it is not an intrinsic component of centrosomes. Intriguingly, the SART1 and PCM proteins, such as γ-tubulin and pericentrin, localize in close proximity but do not overlap. We are not aware of another protein with a similar localization pattern as SART1 at the centrosome periphery. Therefore, we propose this novel centrosomal structure as the SART1 cap, which is potentially important for centrosomal maturation and polar spindle formation. How this cap-like structure forms is an interesting question for the future. We envision that forces moving SART1 toward the cell cortex are important for establishment of the structure.

We found by immunoprecipitation that SART1 interacts with Cep192, the scaffold of centrosome assembly[21,22]. Cep192 depletion in HeLa cells abolishes SART1 accumulation at the spindle poles, whereas SART1 downregulation only partially decreases Cep192 levels at centrosomes. Depletion of either SART1 or Cep192 reduces centrosome staining of several PCM and satellite components. However, whereas Cep192 depletion abolishes γ-tubulin staining at mitotic centrosomes[21,22], SART1 depletion does not impact centrosome localization of this MT nucleation factor (Fig. S6B). Cep192 is known to have dual roles in centrosome duplication and maturation[22]. However, it remains unclear to which extent Cep192 contributes to each function because null mutation or RNAi depletion of Cep192 causes loss of the entire organelle[37]. In contrast to Cep192, depletion of SART1 does not affect the number of centrin dots, indicating that SART1 functions in centrosome maturation but not duplication. These results indicate that although SART1 requires Cep192 for its localization near centrosomes, the downstream functions of SART1 at centrosomes are distinct and probably complementary to that of Cep192.

By immunofluorescence, SART1 is not detectable at centrosomes in interphase but accumulates around centrosomes upon mitotic entry. It is, therefore, surprising that SART1 depletion impairs the localization of centrosomal proteins not only in mitosis but also in interphase. For Ninein, PCM1, EB1 the degree of reduction or scattering is comparable between interphase and mitosis, and even more pronounced reduction of centrosomal staining intensity is observed in interphase for pericentrin. However, SART1 depletion does not reduce mRNA levels of Ninein, PCM1, and Pericentrin, and affect the protein level of EB1, indicating that it does not impair mRNA splicing or protein stability. Thus, it is currently unknown how SART1 regulates their localization but we envision two possible scenarios. First, given the partial localization of SART1 in the interphase cytoplasm[20] (Fig. 2A), small amounts of SART1 beyond the immunofluorescence detection limit may be present at centrosomes in interphase and recruit the centrosomal proteins. Second, SART1 at mitotic centrosomes may act as licensing factor for recruitment of Ninein, PCM1, EB1 and pericentrin in the subsequent interphase.

Similar to RNAi-based knockdown of SART1 in human cells, immunodepletion of SART1 in Xenopus egg extracts causes spindle assembly and chromosome alignment defects, without affecting MT amounts assembled around chromatin. These defects are rescued by expression of exogenous SART1, showing the specificity of the observed phenotypes. Compared to the experiments in human cells, SART1-depleted extracts show more severe defects in spindle pole assembly. This might reflect the larger size (~40 µm in length) of spindles assembled in extracts which results in stronger phenotypes at the places where the depleted protein functions[13]. Alternatively, it might be due to very efficient and rapid depletion setting in egg extracts versus a time demanding downregulation with potential adaptations in cells. Using egg extracts, we further identify the N-terminus of Xenopus SART1 as essential for rescueing the spindle defects. The N-terminus contains a predicted NLS (aa 26-46 of Xenopus SART1[27]). Considering that several nuclear proteins bind to mitotic MTs via their NLS and neighboring redidues[38], we propose that the N-terminus of SART1 is required for spindle pole formation via its MT binding region.

SART1 is overexpressed in various cancer cells[2] but it has been unclear whether the overexpression is a cause or a consequence of tumorigenesis. Our experiments overexpressing SART1 in RPE1 cells did not cause cell transformation, whereas c-Myc expression using a comparable SeV vector transforms these cells. This supports the idea that SART1 overexpression occurs as a consequence of tumorigenesis by reflecting active cell proliferation[2]. On the other hand, downregulation of SART1 efficiently induces programmed cell death in cancer cells but not in normal cells. Upon SART1 downregulation, a considerable number of HeLa cells die after spindle assembly/chromosome alignment defects. Furthermore, SART1 depletion prevents hyperproliferation of RPE1 cells after c-Myc-induced transformation. We imagine that the depletion induces cell death only when RPE1 cells are transformed and this selective cell death prevents tumorigenic-like behavior of cells. It will be interesting and important to understand how cell death is specifically induced in cancer cells. Given that SART1-depleted egg extract shows severe spindle assembly defects and SART1 knockout mice are embryonic lethal[10], differentiated healthy cells may have redundant mechanisms that compensate the loss of SART1. Alternatively, since cancer cells preferentially die with antimitotic drugs taxol and nocodazole[31,39], they

may be sensitive to the downregulation of SART1 required for spindle assembly. In either case, SART1 depletion or inactivation have an impact on cancer proliferation and should be considered as therapeutic strategy.

In summary, our results unravel SART1 as a novel MAP that localizes near centrosomes forming a cap-like structure. Functionally, SART1 promotes recruitment of specific centrosomal components for centrosomal maturation and spindle pole assembly. In addition, depletion of SART1 causes cell death selectively in cancer cell lines establishing SART1 as an attractive target for cancer therapy.

# Methods

### Recombinant proteins and antibodies

A cDNA covering the full-length Xenopus laevis SART1 (NM_001086027.1) was in vitro synthesized (GenScript) and subcloned into pET-28a (Novagen) with NdeI and XhoI sites. For antibody production, the recombinant Xenopus SART1protein was expressed in BL21 (DE3) E. coli and solubilized from inclusion bodies with 6 M urea. The protein was purified with Ni-NTA Agarose (Qiagen), dialyzed to PBS containing 6 M urea, and used for immunization in rabbits (Hokkaido System Science). From the antisera, Xenopus SART1 antibody was purified using the antigen column and used for Western blot at 1 mg/ml. To increase recombinant SART1 solubility, His-Acidic-Target Tag (HisATT), modified from Flag-Acidic-Target Tag[17], was synthesized (Genscript) and subcloned into the above mentioned pET-28a based plasmid with NcoI and NdeI sites. The HisATT-SART1 was expressed in E. coli and purified with Ni-NTA, and dialyzed to CSF-XB buffer (10 mM K-HEPES, 100 mM KCl, 3 mM $MgCl_2$, 0.1 mM $CaCl_2$, 50 mM sucrose, and 5 mM EGTA, pH 7.7) containing 10% glycerol and 1 mM DTT, and used for MT sedimentation assay. For in vitro translation in egg extracts, Xenopus SART1 and its depletion mutants were made by PCR and subcloned into a pCS2+ vector harboring FLAG tag sequence at the N-terminus. Importin a, importin b, and RanQ69L-GTP were expressed in E. coli and purified with TALON beads[15].

The following published and commercial antibodies were used: rabbit (Rb) anti-chTOG[15] for western blot (WB) at 1 mg/ml, Rb anti-α-tubulin[15] for immunofluorescence (IF) at 2 mg/ml, anti-γ-tubulin[30] (Rb, IF 1 mg/ml), Ninein serum[30] (Rb, IF 1:500), PCM1[30] (Rb, IF 1:1000), XCAP-G[16] (Rb, WB 1 mg/ml), a-tubulin (mouse (Ms) B-5-1-2; Sigma, IF 1:2000), BubR1 (Ms, BD, IF 1:500), CENP-A (Ms, Enzo, IF 3 mg/ml), Centrin (Ms, Millipore, IF 1:1000), Cep192 (Rb, Bethyl, IF 1 mg/ml), Cep192 (Rb, GeneTex, used for immunoprecipitation), CREST (human, Antibody Inc., IF 1:200), EB1 (Ms, BD, IF 1:250), FLAG (Ms M2, Sigma, WB 1:1000), g-tubulin (Ms GTU-88, Sigma, WB 1:1000, IF 1:500), GAPDH (Ms, Santa Cruz, WB 1:2000), Ndc80 (Ms, GeneTex, IF 1:500), phospho-Histone H3 (Rb, Millipore, IF 1:500), SART1 #1 (Ms, Abcam, IF 3 mg/ml, WB 1 mg/ml), SART1 #2 (Ms, Santa Cruz, IF 3 mg/ml), and pericentrin (Rb, Abcam, IF 1 mg/ml). Secondary antibodies for immunofluorescence were anti-rabbit IgG conjugated with Alexa Fluor 488, 568, or 647, and anti-mouse IgG conjugated with Alexa Fluor 568 (above from Life technologies, 1:1000), and anti-human IgG conjugated with CF568 (Biotum, 1:1000). DNA was counterstained with DAPI at 1 mg/ml.

## Sendai viruses (SeVs)

Human SART1 mutant resistant to siSART1#3 (s228453) was designed by introducing the following silent mutations into the ORF of SART1 cDNA (NM_005146.5): A813G; T819C; T822C; C825T; C828T. The mutant cDNA with N-terminal FLAG tag was synthesized in vitro (Genewiz), and cloned into pSeV/TSΔF[40] (Fig. S2E). To reconstruct virus, the plasmid DNA was transfected to LLC-MK2 cells stably expressing F (fusion) protein.

## MT binding assays

0.1 μM recombinant SART1 was incubated with 2 μM taxol-stabilized MTs for 15 min, and centrifuged at 20,000 g in a TLA120.2 rotor (Beckman) for 10 min at RT. The Supernatant and pellet was analyzed by Coomassie staining or Western blot. The assay was also done in the presence or absence of recombinant 3 mM importin a, 3 mM importin b, and 5 mM RanQ69L-GTP, a dominant positive mutant of Ran locked in the GTP-bound state.

HeLa nuclear extract (4C Biotech) was diluted to 1 mg/ml with CSF-XB buffer. HeLa nuclear extract (1 mg/ml) was incubated with 2 mM pure taxol-stabilized MTs in the presence or absence of recombinant importin a/b complex and RanGTP, and pelleted. Microtubule-associated proteins (MAPs) were eluted with high salt from the pellet, and the supernatant after a second centrifugation was analyzed by immunoblot.

Xenopus CSF egg extracts were diluted 1:3 with CSF-XB buffer to a concentration of about 30 mg/ml. After centrifugation in a TLA-100.2 rotor at 100,000 x g for 10 min at 4°C, the supernatant was incubated at RT in the presence or absence of 2 μM taxol-stabilized microtubules, 2 μM importin a, 2 μM importin b, and 5 μM RanGTP for 15 min. The samples were centrifuged at 100,000 g for 10 min at 20°C, and pellets were incubated with CSF-XB supplemented with 500 mM NaCl for 5 min, and centrifuged again. The supernatant (eluate) was analyzed by Western blotting.

## Cell Culture, transfection, immunofluorescence, and microscope

HeLa and U2OS cell lines were cultured in Dulbecco's modified Eagle's medium (DMEM) supplemented with 2mM GlutaMAX, 10% FBS and 500 units/ml penicillin-streptomycin (all from Gibco). BJ and RPE1 cells were cultured in MEM (Gibco) supplemented with GlutaMAX, FBS and penicillin-streptomycin as above. RPE1 cells were cultured in DMEM/F12 also supplemented with GlutaMAX, FBS and penicillin-streptomycin. iPS cells were cultured in StemFit (Ajinomoto).

The knockdown experiments were performed with the following siRNA oligonucleotides: siSART1#1 (s17343), 5'-GGCUCAACAUGAAGCAGAAtt-3', siSART1#2 (s17345), 5'-CCCAAUACAGCUUACCGUAtt-3', siSART1#3 (s228453), 5'-CAAUGAUUCUUACCCUCAAtt-3', siCep192 (s226819[23]) (Life Technologies). AllStars siRNA (from Qiagen) was used as negative control. HeLa cells were grown on 12 mm round coverslips (Marienfeld) and transfected with 10 nM of each siRNA using Lipofectamine RNAiMAX

(Invitrogen) according to the manufacturer's instructions. Unless otherwise stated, siSART1#3 was used for the functional analyses of SART1, including the rescue experiment. U2OS, BJ, and RPE1 cells were transfected with 20 nM siRNAs. 72 h after transfection, cells were fixed with Mildform 10N (Wako) at RT for 15 min, washed with PBS, and stored at 4°C.

For rescue experiments, HeLa cells were infected with SeVs at MOI3. After 8 h incubation, medium was replaced to fresh one containing 20 nM siRNAs, and cells were cultured for additional 72 h.

When indicated, HeLa cells were treated with 10 μM taxol or 20 μM nocodazole for 10 min, and fixed with Mildform.

For immunofluorescence staining, cells were incubated with blocking buffer (PBS + 2% BSA + 0.1% Triton-X100) at RT for 30 min, and then incubated with the primary antibodies in the blocking buffer at 4°C overnight. Cells were washed with PBS, incubated with the secondary antibodies and DAPI at RT for 30 min, washed again with PBS, and mounted with Mowiol 4-88 (Calbiochem).

Fluorescence images were acquired by using an Olympus Fluoview FV1000 confocal microscope equipped with a UPlanSApo 60x/1.35 Oil objective at 0.5 μm Z steps. Maximum intensity projections were obtained using ImageJ (NIH). Confocal slices are used to detect kinetochore-MT attachment and sister kinetochore pairs. Interkinetochore distance was measured using ImageJ. Maximum projected images are used to quantify fluorescent intensity using ImageJ. Accumulation of PCM1 at spindles poles was calculated as ratio of PCM1 signal intensity at poles (two 3 μm circles) and larger area around chromatin (10 μm circle) (Fig. 4). Accumulation at interphase centrosomes was calculated as ratio of PCM1 signal intensity at centrosomes (3 μm circle) and larger area around centrosome (10 μm circle) (Fig. 4).

For cell transformation assay, RPE1 cells were infected with SeV harboring SART1 or c-Myc at MOI3 overnight, replaced with fresh medium, and cultured for 1 month with occasional medium change. After fixation with Mildform 10N, cells are imaged by Leica DMIRB bright-field microscope equipped with a N Plan 5x/0.12 objective. To examine the effect of SART knockdown on c-Myc-induced transformation, RPE1 cells were treated with siRNAs and 2 days later infected with SeV harboring c-Myc with MOI3. siRNAs and medium were replaced every 3 days. Cells were fixed in 2 weeks after the first RNAi treatment.

## Live cell imaging experiments

HeLa cells expressing H2B–mCherry were transfected with 20 μM siRNA oligonucleotides in 8-well μ-slide chambers (Ibidi) and, after 24 h, were imaged for 48 h in a Axioobserver Z1 (Zeiss) equipped with a heating and $CO_2$ incubation system (Ibidi), Colobri LED illumination (Zeiss), a CCD camera (AxioCamMR3; Zeiss), and a Plan-Apochromat 10× NA 0.45 M27 objective. Single position files were converted into image sequences with the AxioVision software (LE64; V4.9.1.0; Zeiss). Afterwards, segmentation, annotation, classification of cells were performed using the CellCognition software

(http://www.cellcognition.org/software/cecoganalyzer)[16,18]. More than 100 cell mitotic trajectories per condition were used for quantification and analysis with Microsoft excel and GraphPad Prism.

The wound healing assay was performed using culture-insert 2 well dishes (ibidi, 80206). After 48 h of siRNA treatment in U2OS cells, inserts were removed and cell migration to the vacant zone was imaged every 30 min using a Nikon ECLIPSE Ti2 phase-contrast microscope equipped with a Plan Apo 4x/0.20 objective, 37°C chamber, 5% CO2, and humidity control.

### Flow cytometry

3 day after siRNA transfection, cells were stripped with trypsin and stained with a FITC Annexin V Apoptosis Detection kit (BD) following manufacture's instruction, and analyzed using a CytoFLEX flow cytometer (Beckman Coulter) and FlowJo (FlowJo, LLC).

### Chromosome spreads

HeLa cells were transfected with the indicated siRNAs and grown for 72 h. To enrich mitotic cells, 330 nM nocodazole was added and incubated for 4 h. Cells were stripped by trypsin, washed with PBS, incubated with 75 mM KCl at RT for 8 min. Equal vol of Carnoy's fixative (methanol: acetic acid = 3:1) was added and centrifuged to remove the supernatant. The Carnoy wash was repeated 2 more times. Cells were resuspended in Caynol, spotted on heated slide glass drop by drop, and stained with DAPI for microscopy.

### Quantitative real-time PCR

3 day after siRNA transfection, total RNAs were isolated using PureLink RNA Mini Kit (Ambion) and were subjected to PureLink DNase (Invitrogen) treatment. Reverse transcription and quantitative real-time PCR were conducted using TaqMan RNA-to-Ct 1-step Kit and 7500 Fast Real-Time PCR System (both from Applied Biosystems) with the indicated primer and probe sets (Table S2). To amplify only spliced mRNAs, one of the primers or probe was designed on exon-intron junction. Values were normalized to those of GAPDH.

### Xenopus egg extracts and cell-free assay

Cytostatic factor-arrested M-phase Xenopus laevis egg extracts (CSF extracts) were prepared as described[41]. In short, Xenopus eggs were dejellinated by cysteine treatment, washed with CSF-XB buffer (10 mM K-HEPES, 100 mM KCl, 3 mM $MgCl_2$, 0.1 mM $CaCl_2$, 50 mM sucrose, and 5 mM EGTA, pH 7.7), and crushed by centrifugation at 20,000 g for 20 min in a SW55 Ti rotor (Beckman) at 16°C. The straw-colored middle layer was recovered as a CSF extract. Endogenous SART1 was depleted from CSF extracts by 3 rounds of incubation with 60% (vol/vol) Dynabeads Protein A (Invitrogen) coupled with Xenopus SART1 antibodies.

For spindle assembly in cycled extract[41], CSF extract was supplemented with demembraned sperm, Cy3-labeled tubulin, and 0.4 mM $CaCl_2$, and incubated at 20°C for 90 min to allow cell cycle progression into interphase. Samples were cycled to mitosis by addition a fresh CSF extract and incubation at 20°C for 80 min. MT density around sperm was quantified using ImageJ. For rescue experiments, mRNAs for SART1 full-length and deletion mutants were prepared using mMESSAGE mMachine SP6 kit (Life technologies) and was added to the depleted extract at the beginning of the reactions.

### Immunoprecipitation of SART1 and mass spectrometry

Dynabeads Protein A were coupled with rabbit IgG or the Xenopus SART1 antibody following the manufacturer's instruction. The antibody beads were cross-linked with dimethyl pimelidate. Each bead sample (600 µl slurry) was incubated with Xenopus CSF egg extracts (1000 µl) at 4°C for 60 min, washed twice with CSF-XB and twice with CSF-XB containing 0.5 M KCl and 0.1% Triton X-100. The immunoprecipitates were resuspended in SDS sample buffer and resolved by SDS-PAGE for Coomassie stain or immunoblot.

For shotgun mass spectrometry, the immunoprecipitates (600 µl bead slurry) were eluted from the beads with 0.1 M triethylamine (pH 11.5, 60 µl), and neutralized by addition of final 0.1 M Tris pH 6.8. The proteins were trypsin digested and analyzed with a Q-Exactive mass spectrometer (Thermo Fisher Scientific) at the CoMIT in Osaka University. The peptide data were analyzed by Scaffold (Proteome Software Inc.) and quantitative value was obtained by normalizing total spectra with molecular weight.

For reciprocal immunoprecipitation, human Cep192 antibody (GeneTex) was coupled and cross-linked to Dynabeads Protein A as described above. HeLa cells were cultured to confluence, washed with PBS, and lysed with RIPA buffer (50 mM Tris pH 8.0, 150 mM NaCl, 50 mM sodium orthovanadate, 1% NP40, 0.1 mM PMSF) supplemented with complete protease inhibitor cocktail (Roche). After centrifugation, the total cell lysate (200 µl, ~5 mg/ml) was incubated with the antibody beads (50 µl slurry) at 4°C for 60 min. Beads were washed with the RIPA and resolved by SDS-PAGE for immunoblot.

**Statistical analyses** (describe whether one- or two-tailed)

For live cell imaging, data were tested for normality by D'Agostino and Pearson omnibus test. For normal distributions, ANOVA test and subsequent Dunnett multiple comparisons test were applied. When normal distributions could not be assumed, statistical significance at alpha = 0.001 was determined using a Kruskal–Wallis test followed by Dunn´s multiple comparisons test.

For other fixed cell and egg extract experiments, student´s t-test was performed using Microsoft Excel with two-tail distribution and two-sample equal variance.

# Declarations

### Data Availability

All data of this study are stored at the corresponding author and available on reasonable request. (The source data for the figures are available as a Source Data file.)

### Acknowledgements

We thank Takahiro Maeda, Takayuki Kitogo, Yohei Morita, Yasuji Ueda, Tsuyoshi Tokusumi and Kumiko Saeki for technical advices. This study was supported by JSPS KAKENHI Grant Number JP16K21749 to H.Y.

### Author contributions

K.T. prepared DNA constructs, reconstituted SeVs, and performed RNAi/rescue experiments. J.M. prepared Xenopus SART1 antibody. D.M.A conducted live cell imaging and analysis. Y.H. maintained a frog facility. H.Y. conceptualized and supervised the project, and performed in vitro, human cell and frog egg extract experiments. H.Y. wrote the paper and D.M.A, W.A., and Y.H. revised it.

### Conflict of interest

The authors declare that they have no conflict of interest.

### Materials and Correspondence

Correspondence and material requests should be addressed to Hideki Yokoyama.

## References

1 Shichijo, S. *et al.* A gene encoding antigenic peptides of human squamous cell carcinoma recognized by cytotoxic T lymphocytes. *J Exp Med* **187**, 277-288, doi:10.1084/jem.187.3.277 (1998).

2 Cromer, A. *et al.* Identification of genes associated with tumorigenesis and metastatic potential of hypopharyngeal cancer by microarray analysis. *Oncogene* **23**, 2484-2498, doi:10.1038/sj.onc.1207345 (2004).

3 Olson, J. E. *et al.* Variation in genes required for normal mitosis and risk of breast cancer. *Breast Cancer Res Treat* **119**, 423-430, doi:10.1007/s10549-009-0386-1 (2010).

4 Allen, W. L. *et al.* A systems biology approach identifies SART1 as a novel determinant of both 5-fluorouracil and SN38 drug resistance in colorectal cancer. *Mol Cancer Ther* **11**, 119-131, doi:10.1158/1535-7163.MCT-11-0510 (2012).

5 Makarova, O. V., Makarov, E. M. & Luhrmann, R. The 65 and 110 kDa SR-related proteins of the U4/U6.U5 tri-snRNP are essential for the assembly of mature spliceosomes. *EMBO J* **20**, 2553-2563, doi:10.1093/emboj/20.10.2553 (2001).

6 Kittler, R. *et al.* An endoribonuclease-prepared siRNA screen in human cells identifies genes essential for cell division. *Nature* **432**, 1036-1040, doi:10.1038/nature03159 (2004).

7 Neumann, B. *et al.* Phenotypic profiling of the human genome by time-lapse microscopy reveals cell division genes. *Nature* **464**, 721-727, doi:10.1038/nature08869 (2010).

8 Balestra, F. R., Strnad, P., Fluckiger, I. & Gonczy, P. Discovering regulators of centriole biogenesis through siRNA-based functional genomics in human cells. *Dev Cell* **25**, 555-571, doi:10.1016/j.devcel.2013.05.016 (2013).

9 Sundaramoorthy, S., Vazquez-Novelle, M. D., Lekomtsev, S., Howell, M. & Petronczki, M. Functional genomics identifies a requirement of pre-mRNA splicing factors for sister chromatid cohesion. *EMBO J* **33**, 2623-2642, doi:10.15252/embj.201488244 (2014).

10 Koh, M. Y. *et al.* A new HIF-1alpha/RANTES-driven pathway to hepatocellular carcinoma mediated by germline haploinsufficiency of SART1/HAF in mice. *Hepatology* **63**, 1576-1591, doi:10.1002/hep.28468 (2016).

11 Somma, M. P. *et al.* Moonlighting in Mitosis: Analysis of the Mitotic Functions of Transcription and Splicing Factors. *Cells* **9**, doi:10.3390/cells9061554 (2020).

12 Gruss, O. J. Animal Female Meiosis: The Challenges of Eliminating Centrosomes. *Cells* **7**, doi:10.3390/cells7070073 (2018).

13 Yokoyama, H. *et al.* CHD4 is a RanGTP-dependent MAP that stabilizes microtubules and regulates bipolar spindle formation. *Curr Biol* **23**, 2443-2451, doi:10.1016/j.cub.2013.09.062 (2013).

14 Christodoulou, A. & Yokoyama, H. Purification of nuclear localization signal-containing proteins and its application to investigation of the mechanisms of the cell division cycle. *Small GTPases* **6**, 20-27, doi:10.4161/21541248.2014.978162 (2015).

15 Yokoyama, H. *et al.* The nucleoporin MEL-28 promotes RanGTP-dependent gamma-tubulin recruitment and microtubule nucleation in mitotic spindle formation. *Nat Commun* **5**, 3270, doi:10.1038/ncomms4270 (2014).

16 Yokoyama, H. *et al.* Chromosome alignment maintenance requires the MAP RECQL4, mutated in the Rothmund-Thomson syndrome. *Life Sci Alliance* **2**, doi:10.26508/lsa.201800120 (2019).

17 Sangawa, T. *et al.* A multipurpose fusion tag derived from an unstructured and hyperacidic region of the amyloid precursor protein. *Protein Sci* **22**, 840-850, doi:10.1002/pro.2254 (2013).

18 Held, M. *et al.* CellCognition: time-resolved phenotype annotation in high-throughput live cell imaging. *Nat Methods* **7**, 747-754, doi:10.1038/nmeth.1486 (2010).

19 Li, H. O. *et al.* A cytoplasmic RNA vector derived from nontransmissible Sendai virus with efficient gene transfer and expression. *J Virol* **74**, 6564-6569, doi:10.1128/jvi.74.14.6564-6569.2000 (2000).

20 Binder, J. X. *et al.* COMPARTMENTS: unification and visualization of protein subcellular localization evidence. *Database (Oxford)* **2014**, bau012, doi:10.1093/database/bau012 (2014).

21 Gomez-Ferreria, M. A. *et al.* Human Cep192 is required for mitotic centrosome and spindle assembly. *Curr Biol* **17**, 1960-1966, doi:10.1016/j.cub.2007.10.019 (2007).

22 Zhu, F. *et al.* The mammalian SPD-2 ortholog Cep192 regulates centrosome biogenesis. *Curr Biol* **18**, 136-141, doi:10.1016/j.cub.2007.12.055 (2008).

23 Tsuchiya, Y., Yoshiba, S., Gupta, A., Watanabe, K. & Kitagawa, D. Cep295 is a conserved scaffold protein required for generation of a bona fide mother centriole. *Nat Commun* **7**, 12567, doi:10.1038/ncomms12567 (2016).

24 Delgehyr, N., Sillibourne, J. & Bornens, M. Microtubule nucleation and anchoring at the centrosome are independent processes linked by ninein function. *J Cell Sci* **118**, 1565-1575, doi:10.1242/jcs.02302 (2005).

25 Morrison, E. E., Wardleworth, B. N., Askham, J. M., Markham, A. F. & Meredith, D. M. EB1, a protein which interacts with the APC tumour suppressor, is associated with the microtubule cytoskeleton throughout the cell cycle. *Oncogene* **17**, 3471-3477, doi:10.1038/sj.onc.1202247 (1998).

26 Rodriguez, O. C. *et al.* Conserved microtubule-actin interactions in cell movement and morphogenesis. *Nat Cell Biol* **5**, 599-609, doi:10.1038/ncb0703-599 (2003).

27 Kosugi, S., Hasebe, M., Tomita, M. & Yanagawa, H. Systematic identification of cell cycle-dependent yeast nucleocytoplasmic shuttling proteins by prediction of composite motifs. *Proc Natl Acad Sci U S A* **106**, 10171-10176, doi:10.1073/pnas.0900604106 (2009).

28 Gargini, R., Garcia-Escudero, V., Izquierdo, M. & Wandosell, F. Oncogene-mediated tumor transformation sensitizes cells to autophagy induction. *Oncol Rep* **35**, 3689-3695, doi:10.3892/or.2016.4699 (2016).

29 Leontieva, O. V., Demidenko, Z. N. & Blagosklonny, M. V. Contact inhibition and high cell density deactivate the mammalian target of rapamycin pathway, thus suppressing the senescence program. *Proc Natl Acad Sci U S A* **111**, 8832-8837, doi:10.1073/pnas.1405723111 (2014).

30 Barenz, F. *et al.* The centriolar satellite protein SSX2IP promotes centrosome maturation. *J Cell Biol* **202**, 81-95, doi:10.1083/jcb.201302122 (2013).

31 Brito, D. A. & Rieder, C. L. The ability to survive mitosis in the presence of microtubule poisons differs significantly between human nontransformed (RPE-1) and cancer (U2OS, HeLa) cells. *Cell Motil*

*Cytoskeleton* **66**, 437-447, doi:10.1002/cm.20316 (2009).

32 Momcilovic, O. *et al.* DNA damage responses in human induced pluripotent stem cells and embryonic stem cells. *PLoS One* **5**, e13410, doi:10.1371/journal.pone.0013410 (2010).

33 Lieu, P. T., Fontes, A., Vemuri, M. C. & Macarthur, C. C. Generation of induced pluripotent stem cells with CytoTune, a non-integrating Sendai virus. *Methods Mol Biol* **997**, 45-56, doi:10.1007/978-1-62703-348-0_5 (2013).

34 Mu, R. *et al.* Depletion of pre-mRNA splicing factor Cdc5L inhibits mitotic progression and triggers mitotic catastrophe. *Cell Death Dis* **5**, e1151, doi:10.1038/cddis.2014.117 (2014).

35 Hofmann, J. C. *et al.* The Prp19 complex directly functions in mitotic spindle assembly. *PLoS One* **8**, e74851, doi:10.1371/journal.pone.0074851 (2013).

36 Gerlich, D., Hirota, T., Koch, B., Peters, J. M. & Ellenberg, J. Condensin I stabilizes chromosomes mechanically through a dynamic interaction in live cells. *Curr Biol* **16**, 333-344, doi:10.1016/j.cub.2005.12.040 (2006).

37 Varadarajan, R. & Rusan, N. M. Bridging centrioles and PCM in proper space and time. *Essays Biochem* **62**, 793-801, doi:10.1042/EBC20180036 (2018).

38 Yokoyama, H. Chromatin-Binding Proteins Moonlight as Mitotic Microtubule Regulators. *Trends Cell Biol* **26**, 161-164, doi:10.1016/j.tcb.2015.12.005 (2016).

39 Shi, J., Orth, J. D. & Mitchison, T. Cell type variation in responses to antimitotic drugs that target microtubules and kinesin-5. *Cancer Res* **68**, 3269-3276, doi:10.1158/0008-5472.CAN-07-6699 (2008).

40 Ban, H. *et al.* Efficient generation of transgene-free human induced pluripotent stem cells (iPSCs) by temperature-sensitive Sendai virus vectors. *Proc Natl Acad Sci U S A* **108**, 14234-14239, doi:10.1073/pnas.1103509108 (2011).

41 Hannak, E. & Heald, R. Investigating mitotic spindle assembly and function in vitro using Xenopus laevis egg extracts. *Nat Protoc* **1**, 2305-2314, doi:10.1038/nprot.2006.396 (2006).

42 Luders, J., Patel, U. K. & Stearns, T. GCP-WD is a gamma-tubulin targeting factor required for centrosomal and chromatin-mediated microtubule nucleation. *Nat Cell Biol* **8**, 137-147, doi:10.1038/ncb1349 (2006).

# Figures

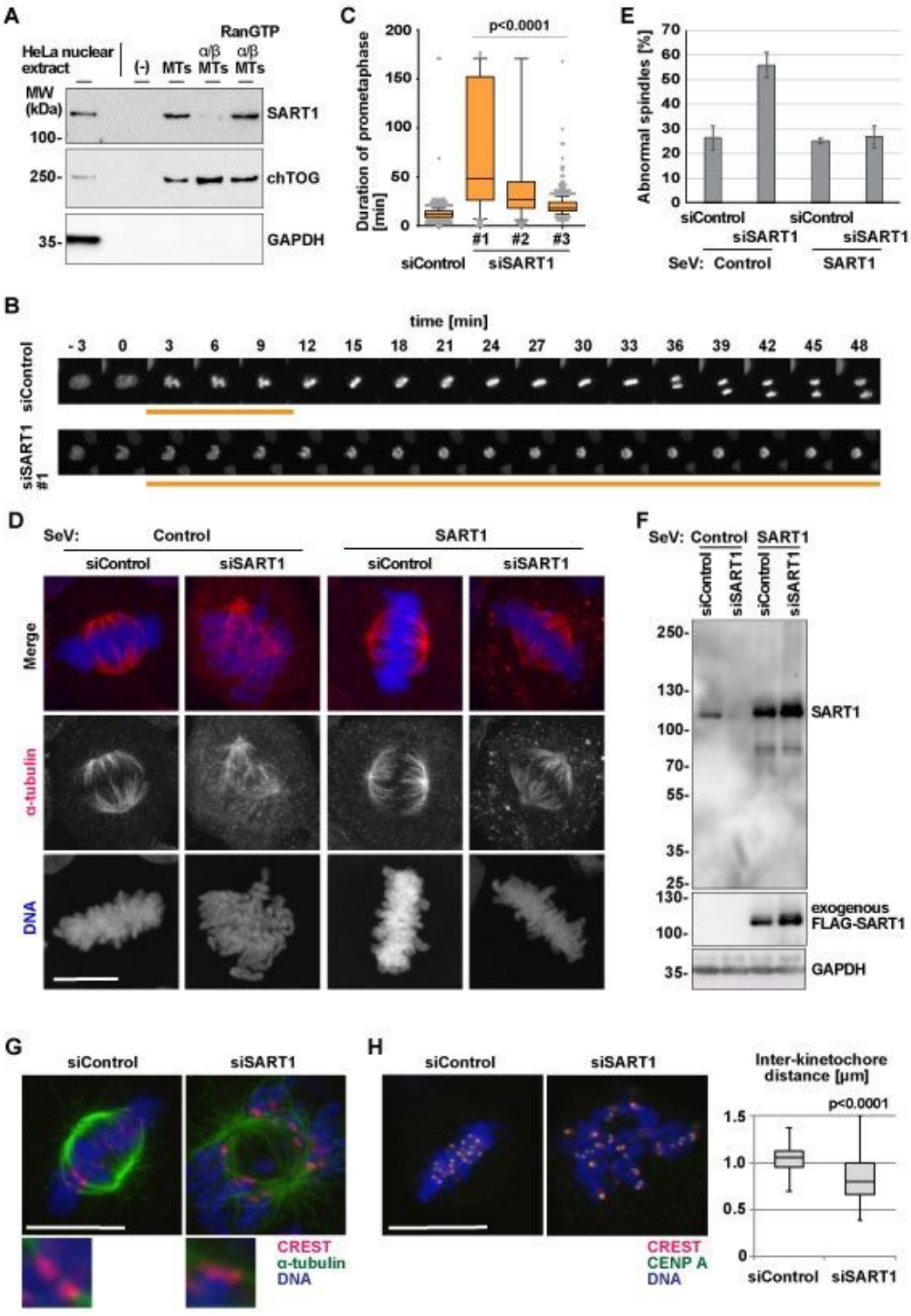


## Figure 1

SART1 is a MAP required for early mitotic progression and spindle assembly. A. Human SART1 binds to microtubules (MTs) in a RanGTP-regulated manner. HeLa nuclear extract was incubated with taxol-stabilized MTs in the presence or absence of recombinant importin a/b complex and RanGTP and pelleted. Microtubule-associated proteins (MAPs) were eluted with high salt from the pellet. After centrifugation, and the supernatant (the eluate) was analyzed by immunobloting. B. HeLa cells

expressing mCherry-H2B were transfected with indicated siRNAs and imaged in intervals of three minutes. Orange lines indicate cells in prometaphase. C. SART1 downregulation extends prometaphase. Duration of prometaphase was quantified for more than 100 mitotic cells per condition. Statistical significance at alpha = 0.0001 was determined using a Kruskal–Wallis test followed by Dunn´s multiple comparisons test. D. SART1 is required for spindle assembly. HeLa cells were infected with control Sendai virus (SeV) vector or SeV carrying an siRNA-resistant version of human SART1. The cells were subsequently treated with control or SART1 siRNAs for 3 days, fixed, stained for α-tubulin and DNA, and imaged by a confocal microscope. Maximum-projected images are shown. E. Quantitation of abnormal spindles assayed in D. Error bars: SD. N = 4 experiments, n > 50 prometaphase and metaphase-like cells were counted per experiment. Note that prophase, anaphase, telophase-like cells were not considered. F. Western blot of lysates from HeLa cells assayed in D. G. MT-kinetochore interactions are compromised upon SART1 downregulation. HeLa cells were treated with the siRNAs, fixed, and stained for the kinetochore marker CREST, α-tubulin, and DNA. Confocal slice images are shown. Note that end-on attachment of MTs to kinetochores are seen in control cells but could not be resolved upon SART1 downregulation. 3-fold magnified images are shown below. H. interkinetochore distance is reduced upon SART1 downregulation. The RNAi-treated cells were stained for the centromere marker CENP-A, CREST, and DNA. Confocal slices were used to find kinetochore pairs and measure interkinetochore distance. n > 94 kinetochore pairs. p values (t-test, two-tailed).Scale bars, 10 mm.

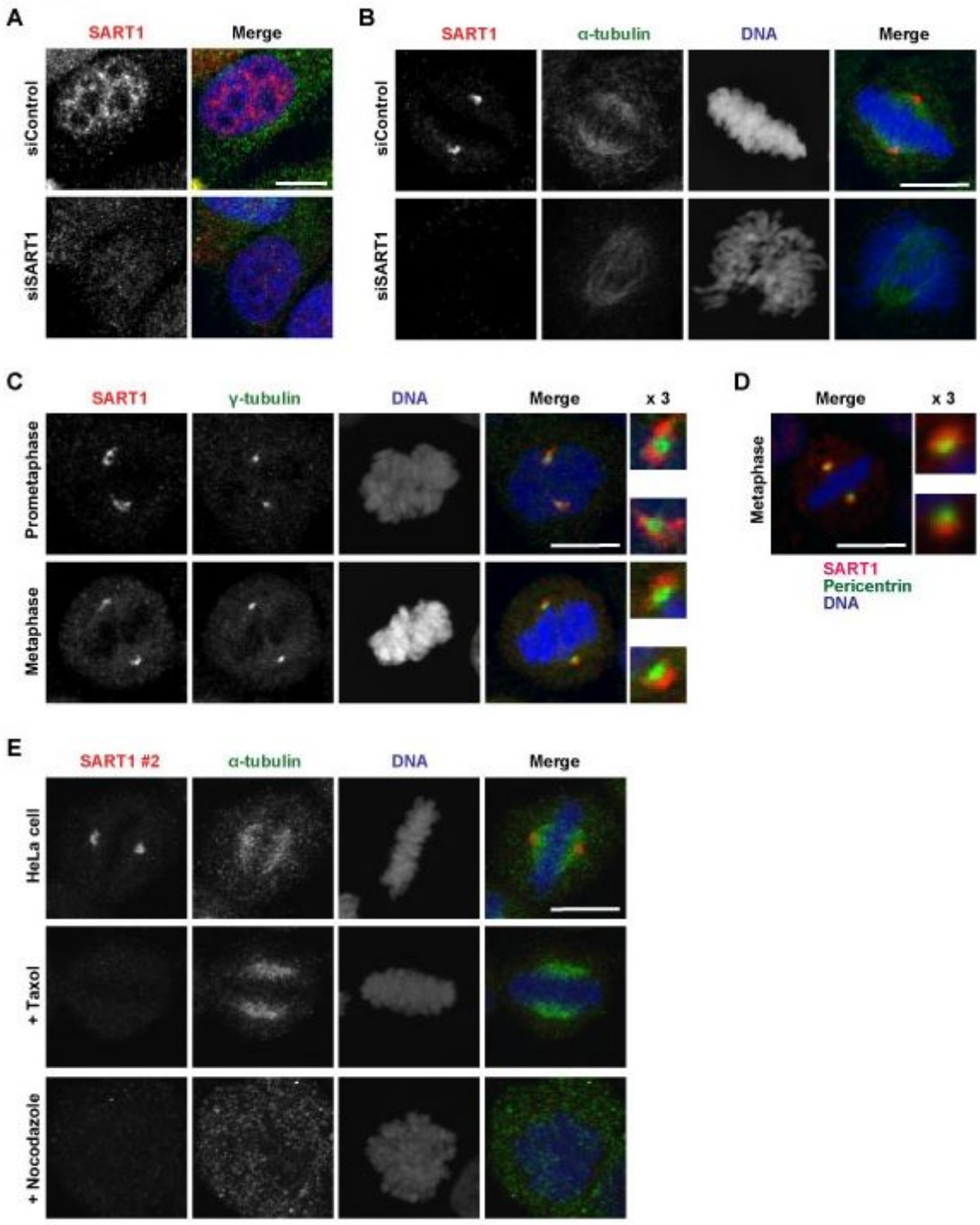


## Figure 2

SART1 localizes to a specific subdomain of mitotic centrosomes. A and B. HeLa cells were treated with control or SART1 siRNAs for 3 days, fixed, and stained for SART1 (red), α-tubulin (green), and DNA (blue). A. In interphase, SART1 localizes within nucleus. B. SART1 localizes to spindle poles. Note that SART1 signals disappear in SART1 RNAi cells, validating the SART1 localization found in control cells. C. HeLa cells were fixed, and stained for SART1, γ-tubulin, and DNA. Note that SART1 localizes around γ-tubulin in early mitosis, but eventually forms a half circle around the γ-tubulin spot distant from the spindle axis. D.

HeLa cells were fixed, and stained for SART1, pericentrin, and DNA. SART1 localizes outside of pericentrin in metaphase. E. The SART1 localization at spindle poles requires dynamic MTs. HeLa cells were treated with excess amount of taxol or nocodazole for 10 min before fixation and stained for SART1 α-tubulin, and DNA. Scale bars, 10 mm.

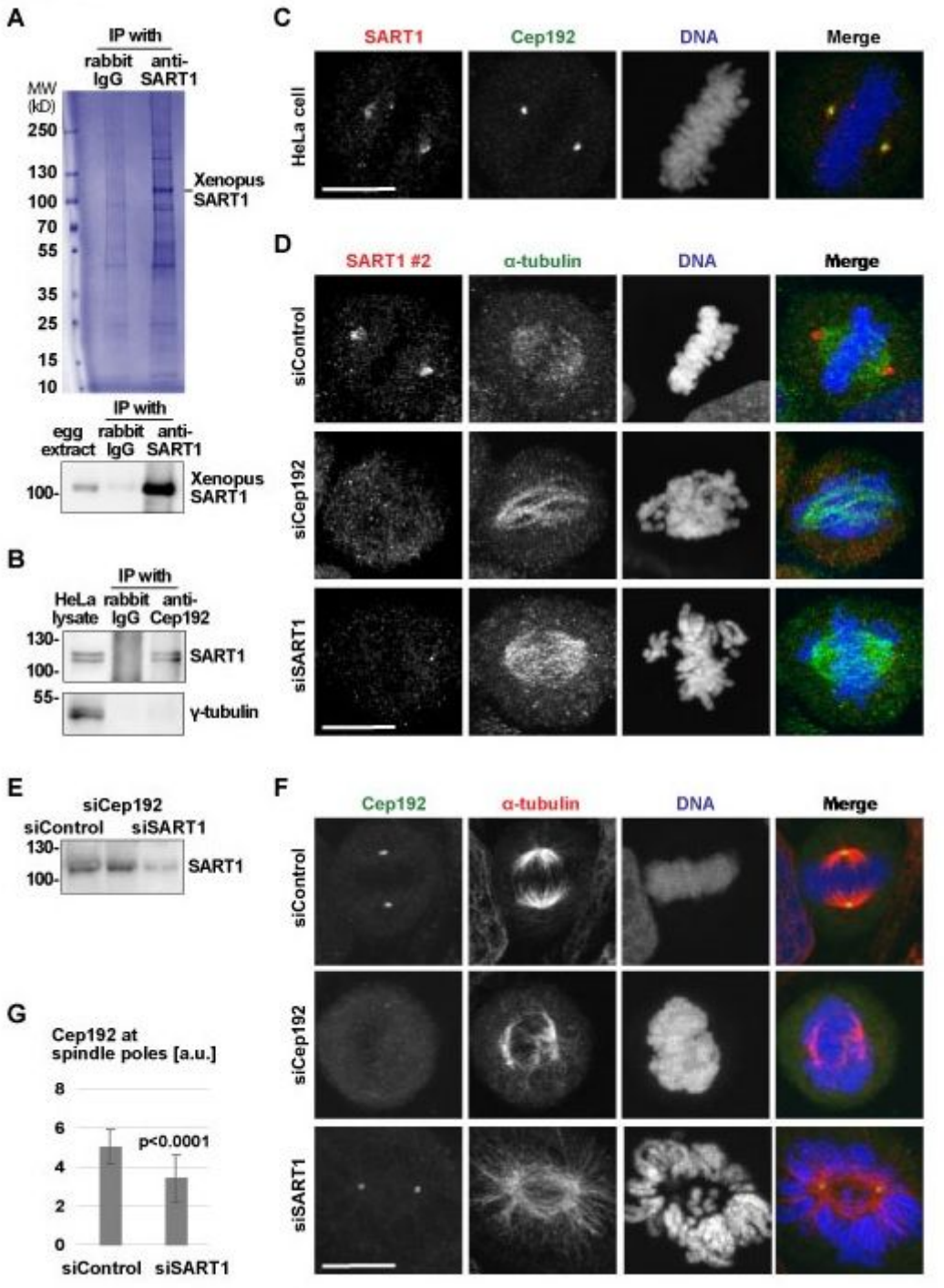


## Figure 3

SART1 localization near centrosomes depends on its interaction partner Cep192 A. Immunoprecipitation (IP) of SART1 from Xenopus egg extract using rabbit polyclonal antibodies raised against Xenopus SART1, analyzed by SDS-PAGE and Coomassie staining. Note the SART1 signal at 110 kDa, confirmed by

Western blot. B. IP from HeLa cell lysate using human Cep192 antibody was analyzed by Western blotting for SART1. γ-tubulin which does not directly interact with Cep19242 serves as negative control. C. SART1 and Cep192 localize close but to distinct structures at metaphase. HeLa cells were immunostained for SART1 and Cep192. DNA was stained with DAPI. D. Cep192 downregulation prevents SART1 localization near centrosomes. HeLa cells were treated with the indicated siRNAs, fixed, and stained for SART1, α-tubulin, and DNA. E. Western blot of cells assayed in D, showing unchanged SART1 levels upon Cep192 downregulation. F and G. SART1 downregulation reduces Cep192 levels at spindle poles. F. siRNA-treated HeLa cells were immunostained as indicated. G. Cep192 levels at the poles were quantified. N = 2 experiments, n = 10 structures per experiment. p values (student's test, two tailed). Note that in siCep192 cells, no centrosomal Cep192 structures are detectable and therefore cannot be quantified. Scale bars, 10 mm.

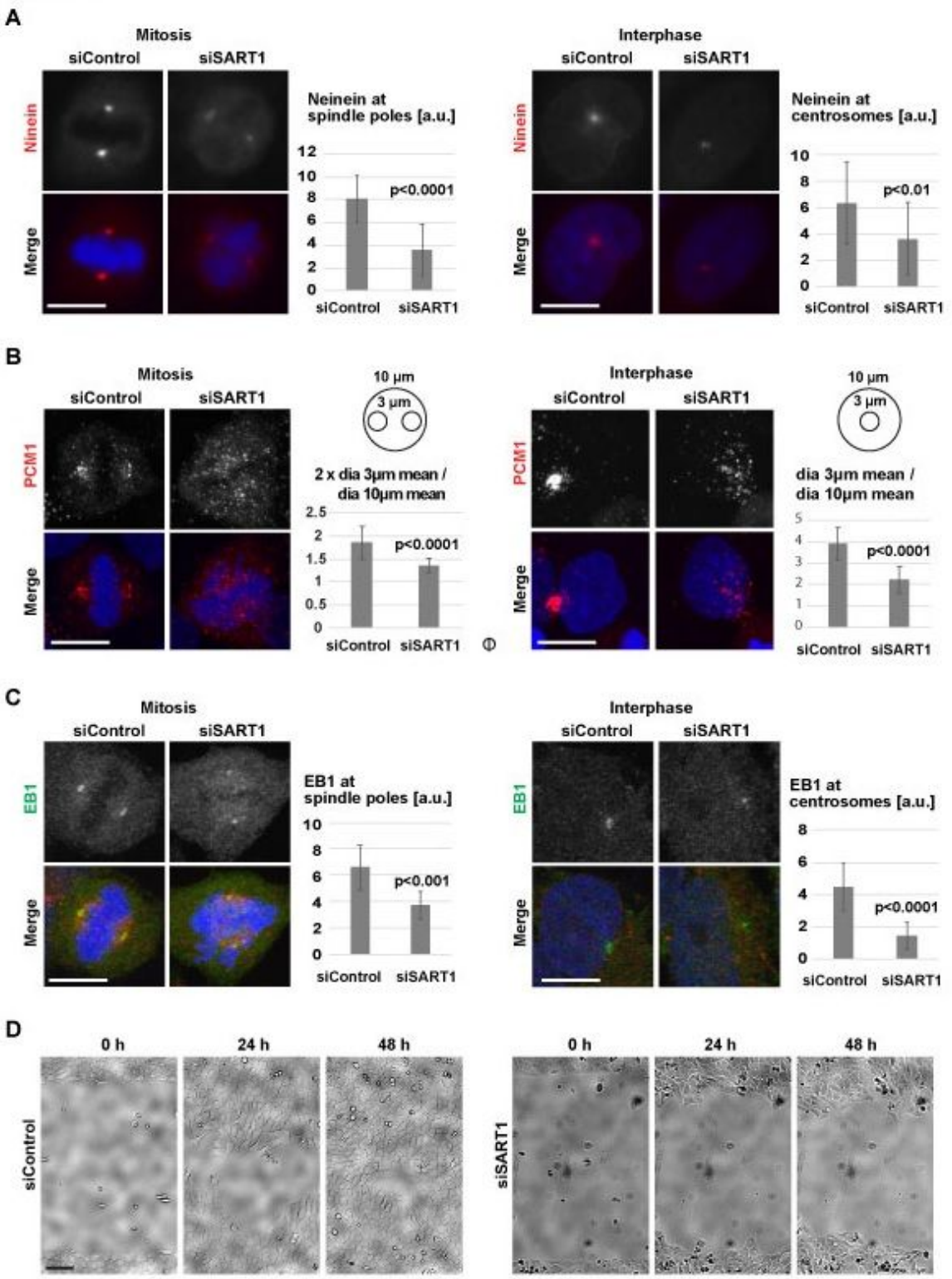


## Figure 4

SART1 is required for recruitment of multiple centrosomal proteins, throughout the cell cycle. A. Centrosomal staining of the pericentriolar material protein Ninein decreases upon SART1 downregulation in mitosis and in interphase. HeLa cells were treated with 10 µM siRNAs for 3 d, fixed, and stained for Ninein and DNA. Ninein intensity at spindle poles and interphase centrosomes were quantified using ImageJ. N = 2 experiments, n = 10 cells per experiment. p values (student's test, two tailed). Scale bar, 10

mm. B. The centriolar satellite protein PCM1 shows a disperse staining pattern upon SART1 downregulation. siRNA-treated HeLa cells were stained for PCM1 and DNA. Accumulation of PCM1 at spindles poles was calculated as ratio of PCM1 intensity at the spindle poles (two 3 µm circles) and a larger area around chromatin (10 µm circle). Accumulation at interphase centrosomes was calculated as ratio of PCM1 intensity at the centrosome (3 µm circle) and a larger area around the centrosome (10 µm circle). N = 2 experiments, n = 10 mitotic structures per experiment. p values (student's test, two tailed). Scale bar, 10 mm. C. EB1 centrosome enrichment is reduced upon SART1 depletion. siRNA-treated cells were stained for EB1 (green), α-tubulin (red), and DNA (blue). EB1 signal at spindle poles and interphase centrosomes was quantified. N = 2 experiments, n = 10 mitotic structures/nuclei per experiment. p values (student's test, two tailed). Scale bar, 10 mm. D. SART1 depletion impairs cell migration. U2OS cells were treated with the indicated siRNAs. Phase-contrast images were taken at indicated times after removing a growth blocking insert from the dish. Scale bar, 100 mm.

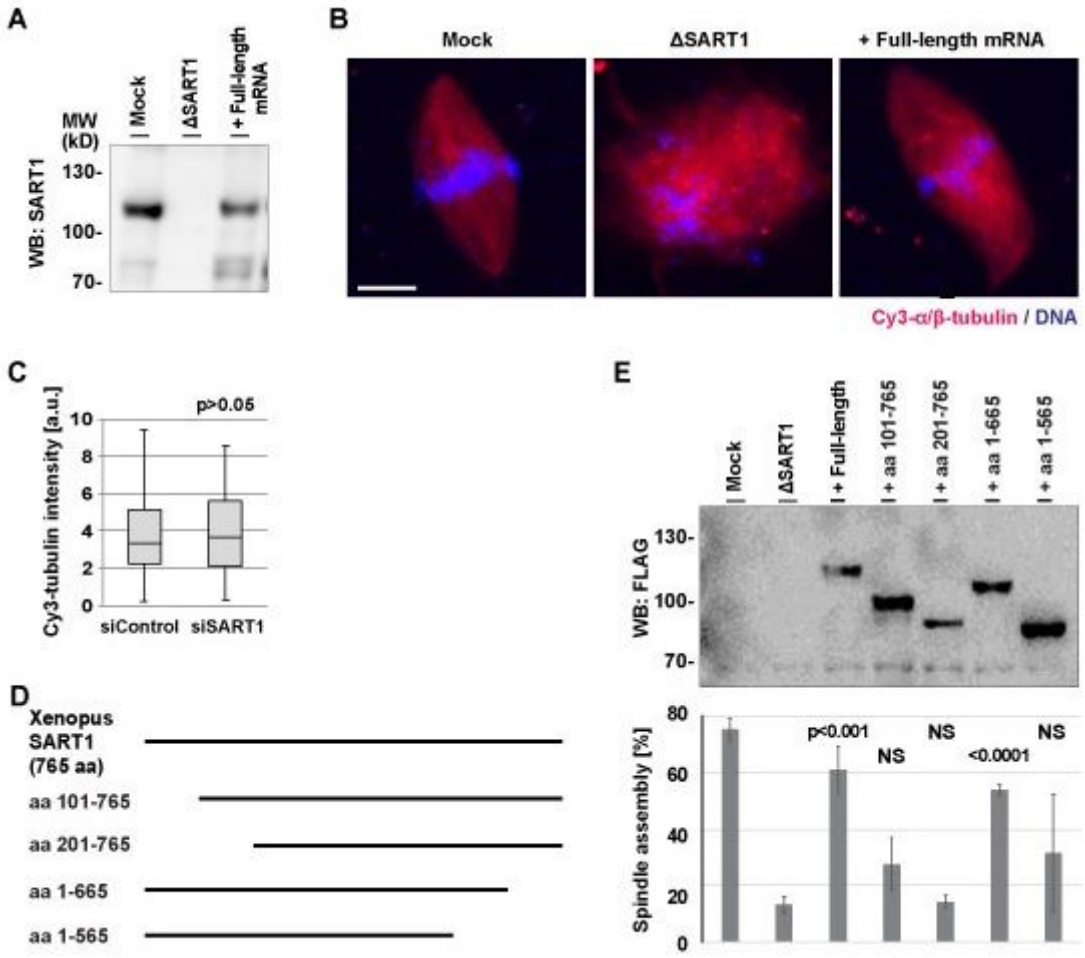


## Figure 5

SART1 is required for spindle assembly in Xenopus egg extracts and its N-terminus is crucial to establish the bipolarity. A. Depletion and addback of SART1, examined by Western blotting. Xenopus laevis egg extract was treated with control (mock) or SART1 antibody-coated beads. The resulting extracts were used for the cell cycle reaction in the presence or absence of SART1 mRNA. B. SART1 is required for

spindle assembly. The extracts shown in A were incubated with sperm, Cy3-labeled tubulin (red) and CaCl2 to induce cell cycle progression to interphase. Further transition to mitosis and spindle assembly was induced by addition of fresh portion of mock or SART1 depleted extracts. DNA was stained with DAPI. Scale bar, 10 mm. C. SART1 depletion does not affect MT amounts assembled around chromatin. Cy3-tubulin intensity around chromatin was quantified. N = 3 experiments, n = 10 structures per experiment. p values (student's test, two tailed). NS (not significant). D. Xenopus SART1 protein and its deletion mutants constructed. E. The N-terminal, NLS-containing region of SART1 is crucial for bipolar spindle assembly. SART1-depleted extract was supplemented with indicated SART1 mRNAs and used for spindle assembly as shown in B. Expression of each exogenous protein was confirmed by Western blot. Frequency of bipolar spindles were counted. N = 3 experiments, n > 50 DNA structures per experiment. p values against ΔSART1 extract (student's test, two tailed). NS (not significant).

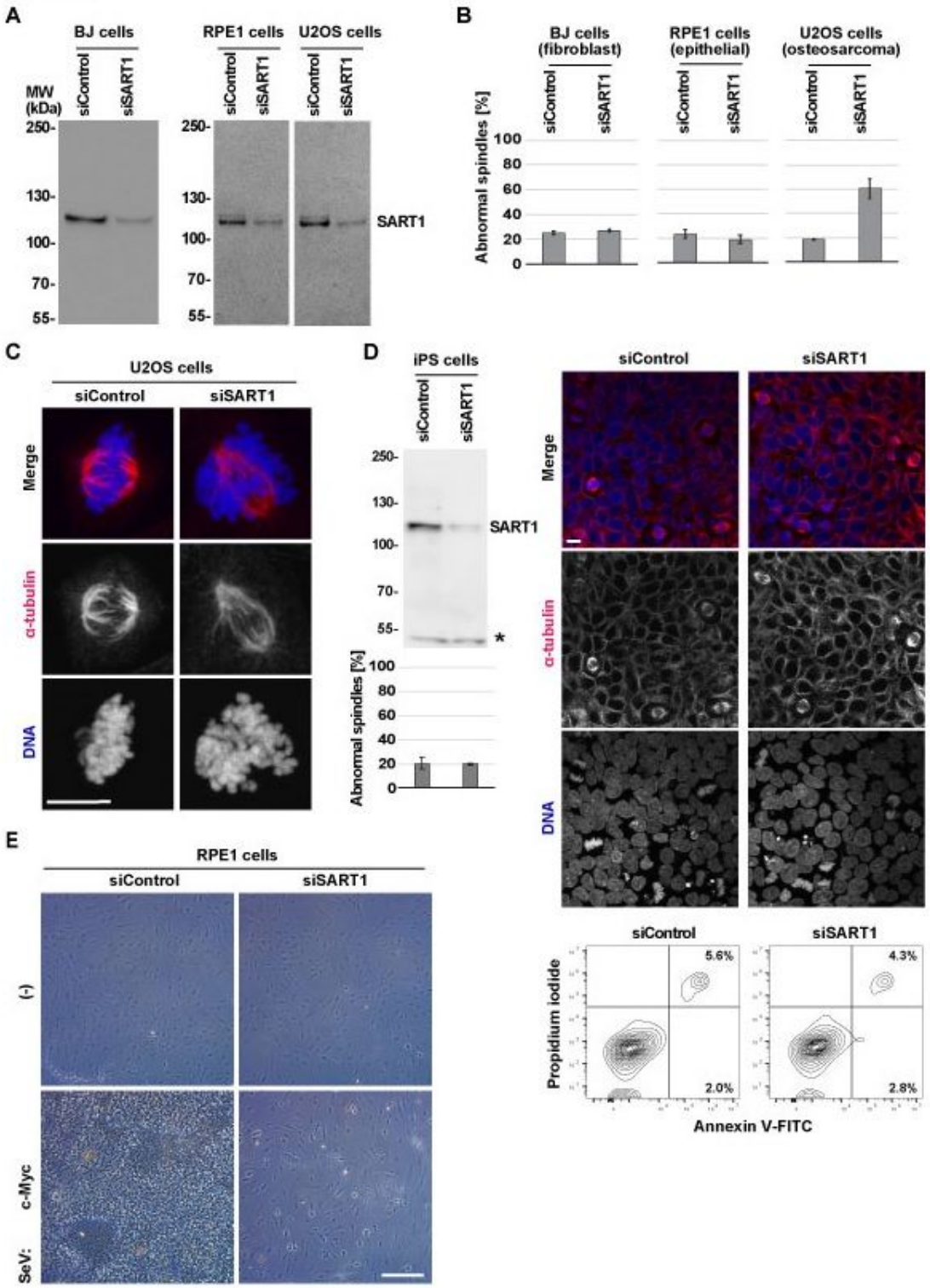


## Figure 6

SART1 depletion causes spindle defects and cell death preferentially in cancer cell lines A. SART1 Western blot analysis of BJ, RPE1, and U2OS cells treated with 20 nM siRNAs for 3 days. B. Cancer-derived U2OS cells show spindle defects upon SART1 downregulation. BJ, RPE1, and U2OS cells treated with siRNAs as in A were stained for α-tubulin and DNA. Abnormal spindle structures were counted as in Fig. 1E. N = 3 experiments, n > 50 prometaphase and metaphase-like cells. C. Representative mitotic

spindles of U2OS cells treated with siRNAs and stained as in B. Scale bar, 10 mm. D. iPS (induced pluripotent stem) cells show normal spindle assembly upon SART1 downregulation. iPS were treated with indicated siRNAs and analyzed for SART1 expression by western blotting. Immunofluorescence analysis and quantitation of spindle assembly defects was done as in B. Flow cytometry analysis showed that SART-depleted cells are viable. Scale bar, 10 mm E. SART1 depletion prevents c-Myc-induced transformation of RPE1 cells. Cells were treated with indicated siRNAs and after 2 days infected with SeV carrying the c-Myc oncogene. siRNAs and medium are replaced every 3 days. Cells were fixed after 2 weeks from the first RNAi treatment.

## Supplementary Files

This is a list of supplementary files associated with this preprint. Click to download.

- Supplementalv1.1.docx
- SupplementaryDataset1.jpg
- SupplementaryDataset2.jpg
- SupplementaryDataset3.jpg
- SupplementaryDataset4.jpg
- SupplementaryDataset5.jpg
- SupplementaryDataset6.jpg
- SupplementaryDataset7.jpg